

JGR Space Physics

RESEARCH ARTICLE

10.1029/2021JA029958

Peter Addison and Lucas Liuzzo contributed equally to this study.

This article is a companion to Liuzzo et al. (2021), <https://doi.org/10.1029/2021JA029740>.

Key Points:

- Based on an analytical model, we study the plasma flow deflection caused by Triton's sub-Alfvénic interaction with Neptune's magnetosphere
- One of Triton's Alfvén wings may be oriented toward upstream, initiating the deflection of the incident flow long before it reaches the moon
- Absorption of the deflected upstream plasma at Triton generates a wake cavity that is displaced away from the moon's geometric plasma shadow

Correspondence to:

S. Simon,
sven.simon@eas.gatech.edu

Citation:

Simon, S., Addison, P., & Liuzzo, L. (2022). Formation of a displaced plasma wake at Neptune's moon Triton. *Journal of Geophysical Research: Space Physics*, 127, e2021JA029958. <https://doi.org/10.1029/2021JA029958>

Received 15 OCT 2021

Accepted 17 DEC 2021

Formation of a Displaced Plasma Wake at Neptune's Moon Triton

Sven Simon¹ , Peter Addison¹ , and Lucas Liuzzo² 

¹School of Earth and Atmospheric Sciences, Georgia Institute of Technology, Atlanta, GA, USA, ²Space Sciences Laboratory, University of California, Berkeley, CA, USA

Abstract A prominent feature of the interaction between a planetary moon and its magnetospheric environment is the formation of a wake cavity in the downstream hemisphere, characterized by a significant decrease of the incident plasma density. Using an analytical model of Triton's sub-Alfvénic interaction with Neptune's magnetosphere, we demonstrate that this moon's wake may be rotated away from its downstream hemisphere into a region that would be accessible to the undisturbed upstream flow. Due to the strong tilt of Neptune's magnetospheric field and the low Alfvénic Mach number of the plasma, one of Triton's Alfvén wings can penetrate into the upstream region and intercept the impinging plasma long before it reaches the moon. The interaction with this upstream wing causes the flow to be deflected toward Triton at a steep angle before being absorbed, thereby generating a wake cavity that is significantly displaced with respect to the moon's geometric plasma shadow. Along the downstream-facing wing, the flow is deflected away from Triton and therefore unable to refill the displaced wake. Since the ionospheric Pedersen conductance greatly exceeds the Alfvén conductance, this asymmetric flow deflection is particularly intense at Triton: when the plasma encounters the wings, it is channeled toward or away from the moon along the axes of the wing tubes. The deflection of the streamlines away from their upstream direction peaks in the range of plasma parameters found along Triton's orbit. Therefore, the displaced wake may be a persistent feature of this moon's plasma interaction and observable during future flybys.

Plain Language Summary Many moons in the outer solar system are embedded in their parent planet's magnetospheres where they are continuously exposed to a flow of magnetized plasma. In general, the partial blockage of this flow by a moon's solid body and ionosphere generates a depletion region at the downstream side where the plasma density is significantly reduced. In addition, the interaction between a moon and its plasma environment triggers non-linear (Alfvén) waves that mainly propagate along the magnetospheric magnetic field. At many large moons of Jupiter and Saturn, the magnetospheric field is nearly perpendicular to the incident flow direction, that is, these waves cannot reach the upstream region. However, Neptune's magnetic field near Triton possesses a strong component along the plasma flow. Therefore, the waves may travel toward upstream and commence deflecting the incident flow before it even comes close to the moon. Since this deflection forces the plasma particles onto highly inclined trajectories toward Triton, their subsequent absorption generates a wake cavity that is no longer located “behind” the moon. Such a displaced wake may be observable during future missions to the Neptune-Triton system and may represent a unique feature in the diverse “zoo” of moon-magnetosphere interaction scenarios at the outer planets.

1. Introduction

Triton, the largest moon of Neptune (radius $R_T = 1,353$ km), is located deep within the ice giant's magnetosphere at a distance of 14.4 Neptune radii ($R_N = 24,622$ km), moving along a highly inclined and retrograde orbit around its parent planet. Similar to many large moons of Jupiter and Saturn, Triton is continuously exposed to a flow of sub-Alfvénic magnetospheric plasma that impinges at a relative velocity of about 40 km/s (Strobel et al., 1990). This magnetized flow sweeps particles out of Triton's ionosphere (Broadfoot et al., 1989; Majeed et al., 1990), generating ramside field pile-up and Alfvén wings in the process (Liuzzo et al., 2021; Strobel et al., 1990). Due to the combination of high ionospheric electron densities in excess of 10^4 cm⁻³ and a weak magnetospheric field along Triton's orbit (3–12 nT, see Connerney et al., 1991), the Pedersen conductance of the moon's ionosphere ($\Sigma_p \approx 10^4$ S) exceeds the Alfvén conductance of the ambient flow ($\Sigma_A \approx 6$ S) by four orders of magnitude (Strobel et al., 1990). Therefore, the interaction between Triton and Neptune's magnetospheric plasma is “saturated,” that is, the streamlines of the impinging plasma are (almost) completely deflected around the Alfvén wing tubes

(Neubauer, 1980, 1998). However, the upstream conditions along Triton's orbit are far more variable in time than the incident plasma parameters at, for example, the Galilean satellites of Jupiter or the largest icy moons of Saturn.

Not only is Neptune's magnetic moment inclined against the planet's rotation axis by 47° , but it is also displaced from the ice giant's center by about $0.55R_N$. In combination with the strong tilt of Triton's orbital plane (157°), this causes substantial variability in the incident magnetospheric plasma conditions. Triton's distance to Neptune's magnetic equatorial plane oscillates between $0R_N$ and $13R_N$, resulting in a change in the ambient field magnitude by about a factor of four and a variability in the upstream plasma density by nearly three orders of magnitude (e.g., Belcher et al., 1989; Ness et al., 1989; Connerney et al., 1991; Mejnertsen et al., 2016). For comparison, the distance of Io and Europa to Jupiter's magnetic equatorial plane changes in time by no more than 1–1.5 planetary radii (Bagenal & Dols, 1989). Most importantly, the angle ξ between the upstream bulk velocity \underline{u}_0 and the ambient magnetospheric field \underline{B}_0 at Triton varies significantly during the course of the moon's orbit. When Triton is located at maximum distance to Neptune's magnetic equatorial plane, both vectors are nearly perpendicular to each other (Liuzzo et al., 2021). Such a configuration represents the "classical" setup of sub-Alfvénic moon-plasma interaction scenarios and provides a very good approximation to capture many key features of the magnetospheric interactions at, for example, Jupiter's Galilean moons and the large icy satellites of Saturn (Kivvelson et al., 2004; Simon et al., 2015). However, whenever Triton comes close to Neptune's magnetic equator, the ambient field components parallel and perpendicular to the upstream flow direction are nearly equal in magnitude (Liuzzo et al., 2021).

Based on the AIKEF hybrid model, Liuzzo et al. (2021) recently studied Triton's magnetospheric interaction for the case of \underline{u}_0 and \underline{B}_0 forming an angle of $\xi = 47^\circ$. Due to the low Alfvénic Mach number of the upstream plasma, the strong tilt of the magnetic field against the flow direction then facilitates the penetration of one of Triton's Alfvén wings into the upstream region. This wing "intercepts" the incident plasma long before the flow reaches the moon (see Figure 1). Such a type of interaction had so far been known only from exoplanets orbiting close to their host stars in a sub-Alfvénic plasma environment (e.g., Saur et al., 2013). As demonstrated by Liuzzo et al. (2021), the impinging magnetospheric flow is deflected toward Triton by the "upstream" Alfvén wing and then partially absorbed by the obstacle (green arrows in Figure 1). Flow deflection within the other Alfvén wing (inclined toward downstream) is directed away from the moon. This hemispheric asymmetry in the flow patterns generates a displaced wake of reduced magnetospheric plasma density (green cylinder in Figure 1) that has only minimal overlap with the "geometric" plasma shadow expected for Triton's downstream hemisphere (red cylinder) and observed at, for example, Tethys and Rhea (Khurana et al., 2008; Simon et al., 2009). With the exception of Titan (where the upstream flow is generally super-Alfvénic), the magnetic field near Jupiter's and Saturn's largest moons does not possess a strong flow-aligned component (see Bertucci et al., 2009; Simon et al., 2010). This is the major reason why such a shifted wake cavity has not yet been observed at any moon in the solar system.

However, the displaced plasma wake identified by Liuzzo et al. (2021) may indeed be a typical feature of Triton's magnetospheric interaction that occurs whenever the inclination angle ξ is smaller than a certain threshold. To corroborate this idea, the goal of our study is to prove analytically that the asymmetric flow deflection pattern proposed as the root cause of the displaced wake is indeed consistent with first principles. In addition, while Liuzzo et al. (2021) considered only two distinct tilt angles ($\xi = 90^\circ, 47^\circ$), we shall apply the analytical approach to systematically investigate the dependence of the flow pattern on the angle between \underline{u}_0 and \underline{B}_0 as well as other key parameters of Triton's sub-Alfvénic interaction.

This study is organized as follows: Section 2 discusses the basic principles of our analytical plasma interaction model. In Section 3 we analyze the flow pattern near Triton's Alfvén wings for different angles between the upstream flow and the magnetospheric field. Section 4 constructs an analytical expression for the "critical" angle between \underline{u}_0 and \underline{B}_0 : if the angle between both vectors is smaller than this threshold, Triton's interaction leads to the formation of the displaced wake cavity. In Section 5, we briefly review our major conclusions and their implications for future exploration of moon-magnetosphere interactions at the ice giants.

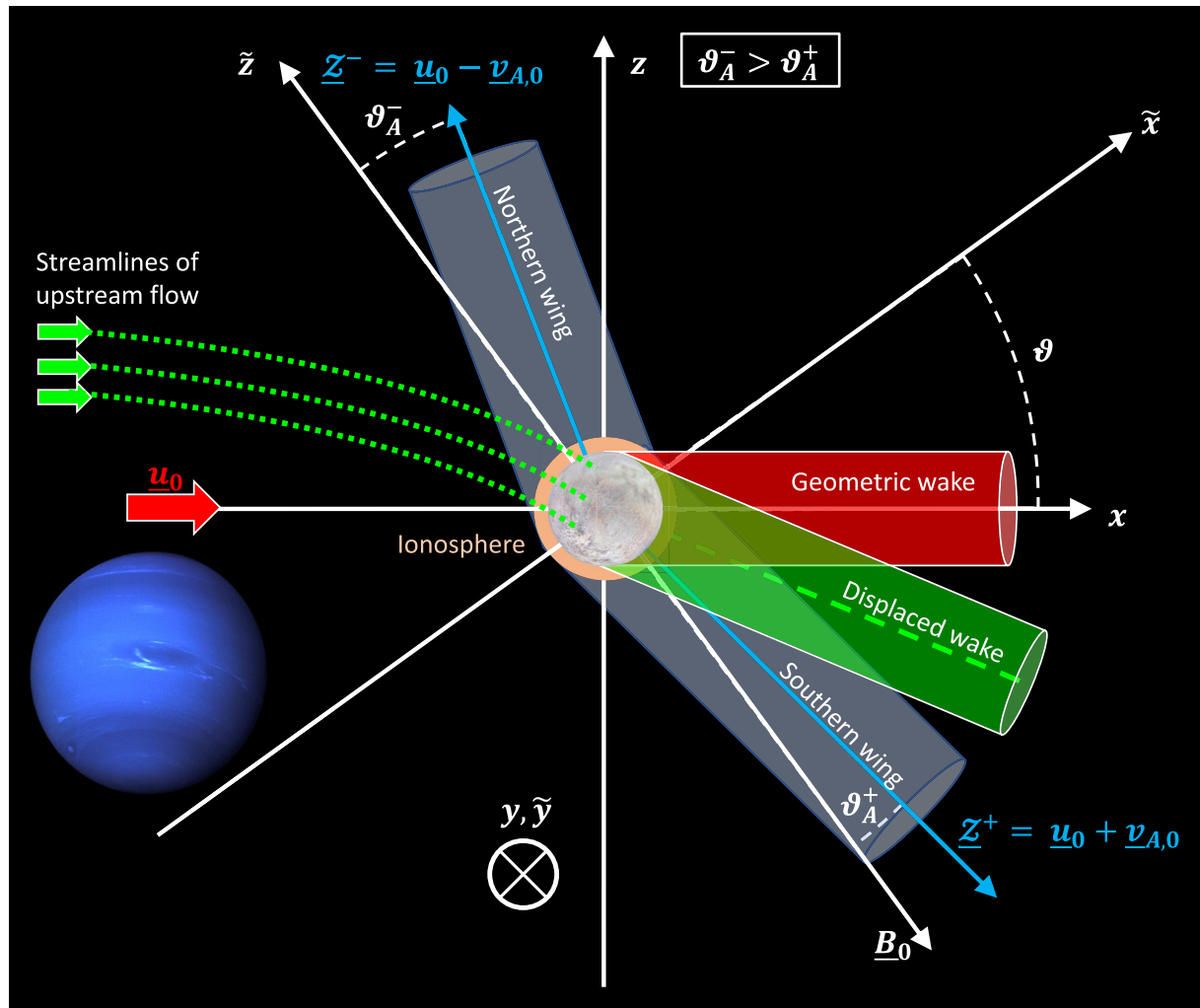


Figure 1. Schematic sketch of the geometry of Triton's interaction with Neptune's magnetospheric plasma. Two Cartesian coordinate systems (x, y, z) and $(\tilde{x}, \tilde{y}, \tilde{z})$ are introduced, both of them centered at Triton. The $(+x)$ axis is aligned with the bulk velocity \underline{u}_0 of the upstream plasma, whereas the $(+\tilde{z})$ axis is antiparallel to the background field \underline{B}_0 . The $(+y)$ and $(+\tilde{y})$ axes are identical and point into the plane of the figure. In both frames, the third axis $(+z)$ or $(+\tilde{x})$ completes the right-handed system. The background field \underline{B}_0 is inclined against \underline{u}_0 by an angle of $\xi = 90^\circ - \vartheta$. Therefore, the angle ϑ_A^\mp between the Alfvén characteristics \underline{z}^\mp (and associated wing tubes, depicted in gray) and \underline{B}_0 is different in the two hemispheres. The undisturbed convective electric field $\underline{E}_0 = -\underline{u}_0 \times \underline{B}_0$ is antiparallel to the y and \tilde{y} axes. In the $z > 0$ hemisphere, the upstream flow (green arrows) is deflected toward Triton by the \underline{z}^- wing and subsequently impinges onto its ionosphere (orange) and surface. This generates a tube-like region of depleted plasma density in the $z < 0$ hemisphere (green) that does not coincide with the moon's geometric plasma shadow (red). The geometric plasma shadow is defined by $\sqrt{y^2 + z^2} \leq R_T$ and $x \geq 0$. While not shown in the figure, the plasma in the $z < 0$ half space is deflected away from Triton and thus, cannot refill the displaced wake. The reader is advised that this schematic illustration does not intend to capture the detailed processes in the near-Triton interaction region where the contribution of transverse ionospheric currents is strong.

2. Model Description

To study the deflection of the magnetospheric plasma near Triton's Alfvén wings, we apply an analytical two-fluid model (electrons and one ion species) originally developed for Io (Saur et al., 1999) and subsequently expanded to capture the physics of dust-plasma interactions at Enceladus (Simon, Saur, Kriegel, et al., 2011; Simon, Kriegel, et al., 2013). More recent versions of this approach were applied to investigate how the non-uniform Pedersen conductance profiles of Enceladus' and Europa's ionospheres map into these moons' Alfvén wings (Simon, 2015; Simon et al., 2021). Here we refrain from reiterating the details of the model setup. For a comprehensive description, the reader is instead referred to the numerous preceding publications (see also Blöcker et al., 2016; Saur, 2004; Saur et al., 2007, 2013).

The model assumes the perturbations of the magnetic field vector $\delta \underline{B} = \underline{B} - \underline{B}_0$ in the moon's Alfvén wings to be small compared to the background field, which is well fulfilled at Triton (Liuzzo et al., 2021). In such a scenario, the *unperturbed* magnetospheric field lines still approximately coincide with the isolines of the electric potential ψ . Therefore, $\psi = \psi(\tilde{x}, \tilde{y})$ depends only on the two coordinates (\tilde{x}, \tilde{y}) perpendicular to the background field \underline{B}_0 (see Figure 1 for the definition of the coordinates). The model captures only the interaction signatures in the Alfvénic far field where the contribution of ionospheric Pedersen and Hall currents to the magnetic field has disappeared. The onset of the flow deflection that gives rise to the displaced wake cavity does indeed occur at a distance of several R_T where Triton's interaction is purely Alfvénic (Liuzzo et al., 2021). The “unknown” quantity in the model is the potential $\psi(\tilde{x}, \tilde{y})$ which can be determined from an ordinary differential equation that requires the moon's ionospheric conductance profile as input. The solution for $\psi(\tilde{x}, \tilde{y})$ then allows to calculate the magnetic field and flow velocity near the Alfvén wings. In other words, while the model does not consider the perturbations generated by transverse ionospheric currents, the currents within the Alfvén wings are still determined by the distribution of conductances within Triton's ionosphere. Since the available model formulations (e.g., Simon, Saur, Kriegel, et al., 2011; Simon et al., 2021) assume the magnetospheric field \underline{B}_0 to be perpendicular to the upstream flow \underline{u}_0 , a few slight modifications are required to make this approach applicable to Triton's variable interaction.

Analogous to the approach of Simon, van Treeck, et al. (2013) for Titan, we introduce a “Triton Interaction” coordinate frame (x, y, z) , see Figure 1. In this system, the magnetospheric background field can be expressed as $\underline{B}_0 = (B_0 \sin \vartheta, 0, -B_0 \cos \vartheta)$ with $B_0 > 0$ and $\vartheta = 90^\circ - \xi$. To maintain consistency with the nomenclature in preceding publications [especially the fundamental work of Neubauer (1980)], we use the angle $\vartheta \in [0^\circ, 90^\circ]$ between the x and \tilde{x} axes that quantifies the deviation from the “classical” case of $\underline{u}_0 \perp \underline{B}_0$. The characteristics of Triton's Alfvén wings are defined by $\underline{z}^\mp = \underline{u}_0 \mp \underline{v}_{A,0}$, with the upper sign referring to the characteristic in the $z > 0$ half space and the lower sign denoting the characteristic in the $z < 0$ half space (Neubauer, 1980). The vector $\underline{v}_{A,0}$ represents the Alfvén velocity in the undisturbed upstream plasma. The plasma and field perturbations are constant along the directions of \underline{z}^\mp , that is, they are not attenuated when moving away from the moon along the characteristics (Neubauer, 1980).

Since \underline{B}_0 possesses a component along the upstream flow direction ($+x$), the Alfvén conductance Σ_A^\mp and the inclination angle ϑ_A^\mp of the Alfvén characteristics against the background field are asymmetric between the two wings. We find

$$\Sigma_A^\mp = \frac{1}{\mu_0 v_{A,0} \sqrt{1 + M_A^2 \mp 2 M_A \sin \vartheta}} \quad \text{and} \quad \sin \vartheta_A^\mp = \frac{M_A \cos \vartheta}{\sqrt{1 + M_A^2 \mp 2 M_A \sin \vartheta}} \quad (1)$$

with the Alfvénic Mach number $M_A = u_0/v_{A,0}$ (see also Neubauer, 1980). The upper and lower signs refer to the \underline{z}^- and \underline{z}^+ wings, respectively. The hemispheric difference in the inclination angles stems from the fact that the upstream velocity possesses a component $u_0 \sin \vartheta$ along the magnetic field \underline{B}_0 . In the \underline{z}^- wing, this component is antiparallel to the group velocity ($-\underline{v}_{A,0}$) of the Alfvén wave. Thus, it reduces the “effective” velocity at which the wave propagates antiparallel to the magnetic field while simultaneously being convected toward downstream perpendicular to the field lines at velocity $u_0 \cos \vartheta$. In the \underline{z}^+ wing, the flow component along the background field increases the “effective” group velocity of the Alfvén wave along the field lines. Therefore, the inclination angle of the wing characteristics against \underline{B}_0 can likewise be expressed as

$$\tan \vartheta_A^\mp = \frac{u_0 \cos \vartheta}{v_{A,0} \mp u_0 \sin \vartheta} = \frac{M_A \cos \vartheta}{1 \mp M_A \sin \vartheta}. \quad (2)$$

Analogous to Equations 1–8 of Simon, Saur, Kriegel, et al. (2011), we obtain generalized expressions for the magnetic field $\underline{B} = (B_{\tilde{x}}, B_{\tilde{y}}, B_{\tilde{z}})$ near the Alfvén wings in the $(\tilde{x}, \tilde{y}, \tilde{z})$ system:

$$B_{\tilde{x}} = \mp \sin \vartheta_A^\mp \sqrt{B_0^2 - (\mu_0 \Sigma_A^\mp)^2 \left\{ \cos^2 \vartheta_A^\mp \left(\frac{\partial \psi}{\partial \tilde{x}} \right)^2 + \left(\frac{\partial \psi}{\partial \tilde{y}} \right)^2 \right\}} \pm \mu_0 \Sigma_A^\mp \cos \vartheta_A^\mp \frac{\partial \psi}{\partial \tilde{y}}; \quad (3)$$

$$B_{\tilde{y}} = \mp \mu_0 \Sigma_A^\mp \cos \vartheta_A^\mp \frac{\partial \psi}{\partial \tilde{x}}; \quad (4)$$

$$B_z = -\cos \vartheta_A^\mp \sqrt{B_0^2 - (\mu_0 \Sigma_A^\mp)^2} \left\{ \cos^2 \vartheta_A^\mp \left(\frac{\partial \psi}{\partial \tilde{x}} \right)^2 + \left(\frac{\partial \psi}{\partial \tilde{y}} \right)^2 \right\} - \mu_0 \Sigma_A^\mp \sin \vartheta_A^\mp \frac{\partial \psi}{\partial \tilde{y}}. \quad (5)$$

The Alfvénic nature of these magnetic signatures is readily verified: $|\underline{B}| = B_0$. The magnetic field components in the (x, y, z) system then read

$$B_x = B_{\tilde{x}} \cos \vartheta - B_z \sin \vartheta; \quad (6)$$

$$B_y = B_{\tilde{y}}; \quad (7)$$

$$B_z = B_{\tilde{x}} \sin \vartheta + B_z \cos \vartheta. \quad (8)$$

The flow velocity \underline{u} near the Alfvén wings can be obtained from

$$\underline{u} = \underline{u}_0 \pm \frac{\underline{B} - \underline{B}_0}{\sqrt{\mu_0 n_0 m}} = \underline{u}_0 \pm \frac{\delta \underline{B}}{\sqrt{\mu_0 n_0 m}}, \quad (9)$$

where m and n_0 denote the ion mass and number density of the undisturbed upstream plasma (see Equation 23 in Simon et al., 2021). Since the flow in the Alfvénic far field is incompressible, the plasma density in that region has a constant value n_0 (Neubauer, 1980). In other words, acceleration by pressure gradient forces (which may occur close to Triton) is not taken into account by our model.

Since the perturbations of the upstream flow are assumed to be weak, the Alfvén wing tubes in the model are (approximately) centered around the $(\pm \tilde{z})$ axis (Simon, Saur, Kriegel, et al., 2011; Simon et al., 2021; Simon, Kriegel, et al., 2013; Simon, 2015). Therefore, inserting Equations 3–5 into Equation 9 immediately reveals that the interaction perturbs the velocity component u_z along the Alfvén wings, in addition to the perturbations in $u_{\tilde{x}}$ and $u_{\tilde{y}}$ that correspond to the deflection of the upstream flow around the wing tubes [see Figures 2 and 3 of Simon et al., 2021]. The flow perturbations along the wing characteristics are generated by the currents associated with the sub-Alfvénic interaction. As shown by Neubauer (1980), an Alfvén wing carries two distinct current systems that are completely decoupled from each other: the first of these systems is directed along the wing characteristics and ultimately connects the moon to its parent planet's ionosphere (e.g., Hess et al., 2011). The second system encircles the wing tubes in closed loops, with the associated magnetic perturbations ensuring the constancy of $|\underline{B}|$. Applying the right-hand rule to these loop-like currents shows that they generate magnetic perturbations along the $(\pm \tilde{z})$ axis, similar to the field inside a coil. According to Equation 9, these wing-aligned magnetic perturbations then map into a velocity component of the deflected flow parallel or antiparallel to the characteristics.

For our model calculations, we adapt the upstream conditions from Table 1 of Liuzzo et al. (2021): Triton is exposed a flow of singly charged magnetospheric ions with average mass $m = 7.5$ amu and number density $n_0 = 0.11 \text{ cm}^{-3}$, impinging onto the moon at a relative velocity of $u_0 = 43$ km/s. The magnitude of the magnetospheric background field is set to $B_0 = 5.14$ nT and the field vector is assumed to be parallel to the (x, z) and (\tilde{x}, \tilde{z}) planes. While the $\vartheta = 43^\circ$ simulation of Liuzzo et al. (2021) did include a magnetic field component $B_{0,y} \neq 0$ perpendicular to these planes, its value was a factor of 200 weaker than the components parallel to them. In general, a non-zero $B_{0,y}$ component of the background field can always be eliminated by rotating the Triton Interaction System around the x axis, that is, confining \underline{B}_0 to the (x, z) plane does not limit the validity of our results. Our choice of parameters yields an Alfvénic Mach number of $M_A = 0.35$ for the upstream flow. The angle ϑ is treated as a free parameter. At Triton, the expected values of ϑ range from (-43°) to $(+43^\circ)$ (see Liuzzo et al., 2021). However, in this study we consider the range $0^\circ \leq \vartheta \leq 90^\circ$. A negative value of ϑ would merely flip the key features of the interaction between the two hemispheres (see Section 4 for details). The $z < 0$ wing would then penetrate into Triton's upstream hemisphere and the displaced wake could be found in the $z > 0$ half space. Also, taking into account ϑ values up to 90° (i.e., \underline{u}_0 and \underline{B}_0 are aligned) will allow us to provide context for the physics of the displaced wake observable at Triton.

We consider the plasma interaction with Triton's ionosphere alone, that is, our model does not take into account the contribution of an induced field from a possible (but yet unobserved) subsurface ocean (e.g., Saur et al., 2010), nor any induction signal from the moon's ionosphere (see Hartkorn and Saur, 2017). In the Alfvénic far field, such an induced field would generate a slight shrinkage of the Alfvén wing tubes and a displacement

away from an axis through Triton's center (Neubauer, 1999; Volwerk et al., 2007). However, it would not cause any qualitative changes of the flow pattern near the wings: while the model of Liuzzo et al. (2021) does take into account an induced field, the displaced wake (and associated deflection pattern of the plasma) are clearly discernible in their results.

3. Wake Formation at Triton

To illustrate how deviations from $\underline{u}_0 \perp \underline{B}_0$ affect the flow deflection near Triton's Alfvén wings, we first evaluate the electric potential ψ for a realistic, "suspension bridge"-like profile of the Pedersen conductance Σ_p in the moon's ionosphere (see Blöcker et al., 2016; Neubauer, 1998; Simon, 2015; Simon et al., 2021 for details). Hence, the value of Σ_p maximizes along the bundle of magnetospheric field lines tangential to Triton's surface and achieves a local minimum in the region where \underline{B}_0 is perpendicular to the obstacle. In agreement with the estimations of Strobel et al. (1990), the average Pedersen conductance in the model ionosphere is set to $\langle \Sigma_p \rangle \approx 4.5 \cdot 10^4$ S. The radius of the obstacle to the flow is $R = R_T + 3H$, with $H = 70$ km approximately representing the scale height of Triton's atmosphere (Broadfoot et al., 1989). The inclusion of a realistic shape for the ionospheric Pedersen conductance profile comes at the expense of having to set the Hall conductance to $\Sigma_H = 0$ (Simon, 2015; Simon et al., 2021). However, this limitation does not affect our conclusions since the Hall effect would merely introduce a rotation of the flow pattern in planes *perpendicular* to the wing characteristics, that is, it would only break the symmetry between the $y > 0$ and $y < 0$ hemispheres (Saur et al., 1999; Simon, Saur, Kriegel, et al., 2011; Simon, Kriegel, et al., 2013). The center of the displaced wake would then be moved out of the $y = 0$ plane. Besides, the range of Σ_H values at Triton has not yet been constrained through modeling or observations.

Figure 2 displays the resulting u_z component of the bulk velocity (in Triton Interaction coordinates) along cuts through the \underline{z}^- (left column, $z > 0$) and \underline{z}^+ (right column, $z < 0$) wings at $z = \pm 3R_T$ for three different values of ϑ . In each plot, the plateau-like region of nearly constant u_z corresponds to the "interior" of the wing tubes. As can be seen from the first row of Figure 2, when \underline{u}_0 and \underline{B}_0 are perpendicular to each other, the u_z component of the flow velocity points *away* from the moon in both hemispheres: u_z is positive in the $z > 0$ wing [panel 2(a)] and negative in the $z < 0$ wing [panel 2(b)]. This is the scenario that occurs at, for example, the Galilean moons, Dione, and Rhea (e.g., Kivelson et al., 2009; Simon, Saur, Neubauer, et al., 2011; Simon et al., 2012; Liuzzo et al., 2016). Introducing a minor deviation of $\vartheta = 6^\circ$ from this "ideal" case, the u_z component in the $z < 0$ wing remains negative, but increases in magnitude by about a factor of 1.5 [panel 2(d)]. However, in the $z > 0$ hemisphere u_z is positive only within the (plateau-like) inner region of the Alfvén wing, whereas the flow near its outer edges has switched directions ($u_z < 0$) and now possesses a component *toward* Triton [panel 2(c)]. This deflection toward Triton is still a factor of 3 weaker than the motion away from the moon within the wing tube.

Further increasing the angle to the value of $\vartheta = 43^\circ$ used by Liuzzo et al. (2021) goes along with a complete reversal of the flow direction within the $z > 0$ wing: the flow in *both* wings now has a component antiparallel to the z axis, that is, toward Triton in the $z > 0$ hemisphere and away from the moon in the $z < 0$ hemisphere [panels 2(e) and (f)]. The negative u_z component of the flow velocity in the $z > 0$ wing becomes as large as $\approx 50\%$ of the upstream value u_0 . In the $\vartheta = 43^\circ$ scenario, Triton's $z > 0$ Alfvén wing has completely moved into the upstream hemisphere ($x < 0$) and is therefore able to deflect the flow before it reaches the moon. The resulting flow pattern facilitates the formation of the "displaced" wake: in the $z > 0$ hemisphere the plasma is directed toward Triton and is partially absorbed, while the deflected flow in the $z < 0$ hemisphere is unable to replenish the emerging wake cavity (see also Liuzzo et al., 2021). In all three cases studied, the $z < 0$ wing remains tilted toward downstream ($x \geq 0$), and the associated u_z perturbation is consistently negative. The deflection of the flow in ($-z$) direction is *not* restricted to the "inner" regions of the wing tubes (see Figures 2e and 2f): as shown by Neubauer (1980), the magnetic field and flow perturbations decrease with $1/\tilde{r}^2$, where \tilde{r} denotes the distance to the respective wing axis. Therefore, the proposed deflection mechanism still operates at a certain distance to the wings, albeit attenuated in magnitude.

As can be seen from Figure 3, the flow pattern from the $\vartheta = 43^\circ$ scenario (Figures 2e and 2f) qualitatively matches many predictions of the AIKEF hybrid model: in large regions of the $z > 0$ and $z < 0$ half spaces, the u_z component is negative. However, within the displaced wake, the analytical model suggests a negative u_z component (which would be blue in Figure 3b), whereas the flow in the AIKEF output is deflected *toward* Triton ($u_z > 0$, red in Figure 3b). Such a deviation between the AIKEF results and the analytical model is expected. First, the analytical

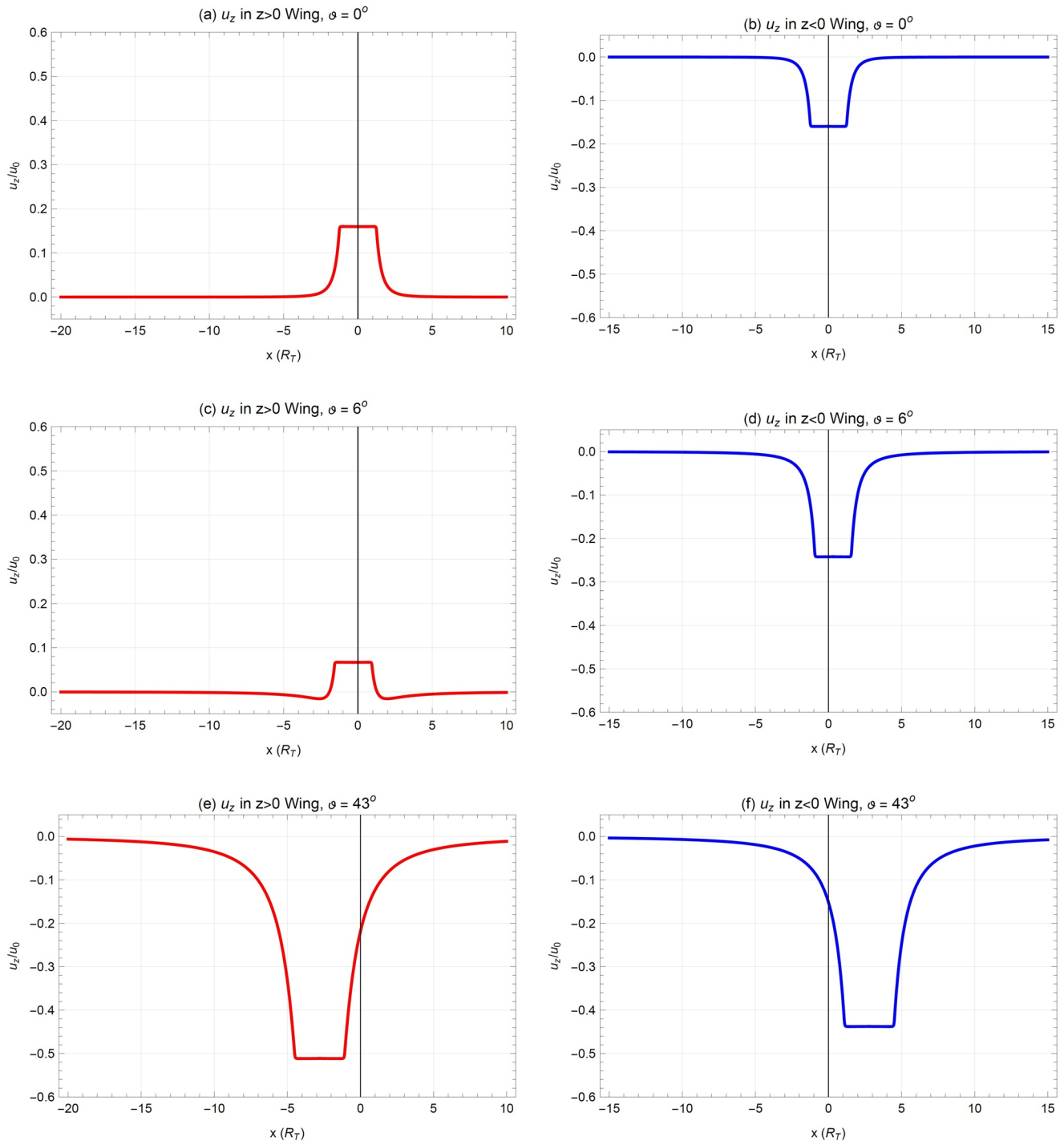


Figure 2. Flow deflection in Triton's Alfvén wings. For different angles $\theta = 0^\circ$ (a and b), $\theta = 6^\circ$ (c and d), and $\theta = 43^\circ$ (e and f), the figure displays the north-south component u_z of the plasma bulk velocity along “horizontal” cuts through the Alfvén wings at $y = 0$, $z = +3R_T$ (left) and $y = 0$, $z = -3R_T$ (right). The values of u_z are normalized to the upstream velocity u_0 .

model is strictly applicable only at large distances to Triton where the tail formed by ionospheric pick-up ions no longer contributes to the perturbations. However, pick-up ion gyroradii at Triton are comparable to the radius of the moon (Liuzzo et al., 2021), and almost the entire downstream region within the AIKEF domain is therefore “filled” with newly generated ionospheric particles (see Figure 7 of Liuzzo et al., 2021). Second, the analytical model does not capture any density gradients in the plasma and their feedback on the electric field. Near Triton,

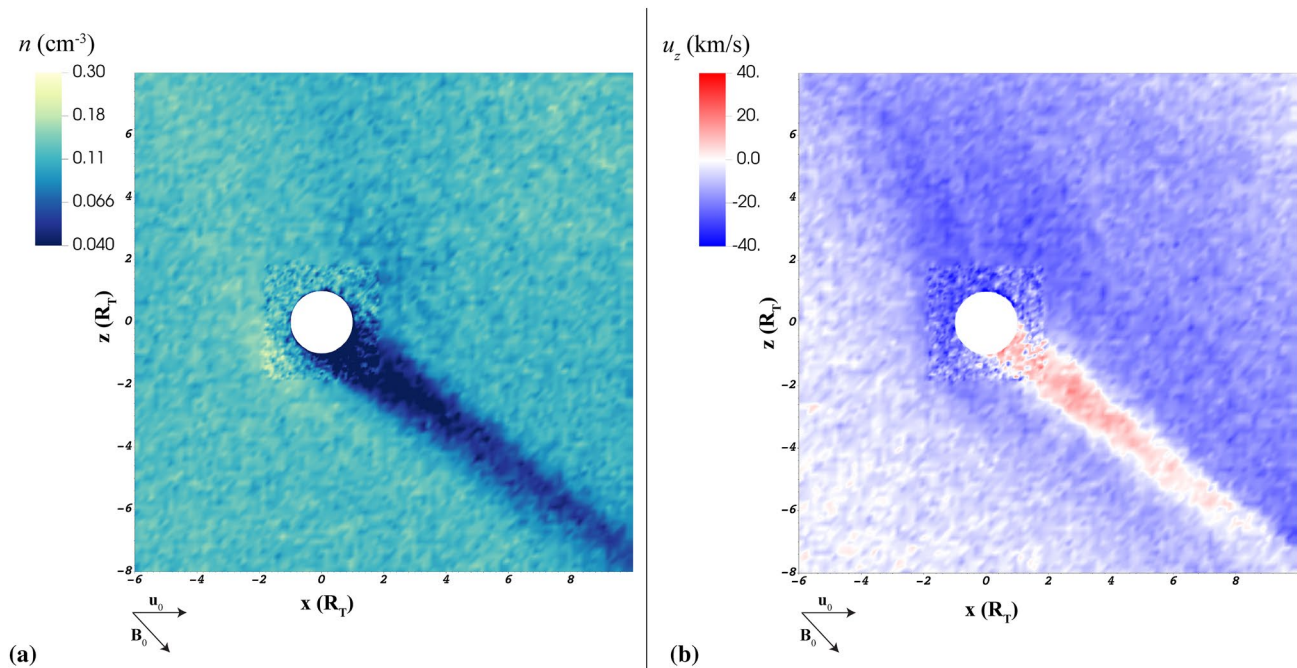


Figure 3. (a) Number density of the magnetospheric upstream plasma and (b) u_z component of the upstream flow velocity in the (x, z) plane, as obtained from the AIKEF hybrid model (Liuzzo et al., 2021). The results shown here are from the same AIKEF run as discussed in Section 3.2.2 of our companion paper; only the coordinate system has been adjusted to match the nomenclature used in this manuscript.

such gradients are generated not only by the inflated pick-up tail, but also by the displaced plasma wake itself (see Figure 3a). The pressure gradients associated with the displaced wake are responsible for accelerating a portion of the adjacent flow back into the density void, thereby causing a reversal in the sign of u_z in the segment of the wake close to Triton (red in Figure 3b). However, this effect is only subtle and *not* able to refill the displaced wake (see Figure 3a). In other words, despite the high velocity calculated by AIKEF within the displaced wake, this velocity is associated with only a small number of particles. Therefore, this particular aspect of the AIKEF output is *not* a contradiction to the analytical results. Third, the thermal velocity of the magnetospheric ion population incident upon Triton exceeds the upstream flow speed u_0 . Hence, particles with velocity vectors away from the $(+x)$ direction significantly contribute to shaping the interaction signatures in the vicinity of the moon (e.g., Simon et al., 2007). This effect is not captured by the fluid approach of our analytical model. For these reasons, there are non-negligible differences between the output of the analytical model (for the far field) and the perturbations of flow and magnetic field produced by AIKEF in the immediate vicinity of Triton [see also discussion of Equations 7–9 in Liuzzo et al. (2021)].

4. Critical Angle for Flow Deflection

Figure 2 suggests the existence of a "critical" angle ϑ_c at which the sign of u_z within the $z > 0$ wing tube flips from plus to minus. Our goal is to determine a simple analytical expression that links ϑ_c to the key parameters of Triton's sub-Alfvénic interaction. For this purpose, we proceed analogous to, for example, Saur et al. (1999); Saur et al. (2007, 2013), Simon, Saur, Kriegel, et al. (2011), and Simon, Kriegel, et al. (2013): introducing polar coordinates $(\tilde{r}, \tilde{\phi})$ in planes perpendicular to the background field \underline{B}_0 , we treat the obstacle to the flow as a cylinder of radius $\tilde{r} = R$ and constant Pedersen conductance $\Sigma_p = \langle \Sigma_p \rangle$. Again not considering the ionospheric Hall effect, the electric potential ψ can then be expressed as

$$\psi = \psi^{\mp}(\tilde{r}, \tilde{\phi}) = \begin{cases} E_0 \alpha^{\mp} \tilde{r} \sin \tilde{\phi} & \tilde{r} \leq R \\ \frac{E_0 R^2}{\tilde{r}} \gamma^{\mp} \sin \tilde{\phi} + E_0 \tilde{r} \sin \tilde{\phi} & \tilde{r} > R \end{cases}, \quad (10)$$

where $E_0 = u_0 B_0 \cos \vartheta$ represents the undisturbed convective electric field (see Equations 62 and 65 in Simon, Saur, Kriegel, et al., 2011). The four constants α^\mp and γ^\mp follow from the continuity of the potential at $\tilde{r} = R$ and the boundary condition (A2) from Saur et al. (1999); they read

$$\alpha^\mp = \frac{2\Sigma_A^\mp}{\Sigma_P + 2\Sigma_A^\mp} \quad \text{and} \quad \gamma^\mp = \alpha^\mp - 1. \quad (11)$$

The quantity $\lambda^\mp \equiv 1 - \alpha^\mp$ is often referred to as the "interaction strength", as it becomes unity for $\Sigma_P \gg \Sigma_A^\mp$ and vanishes for $\Sigma_P \ll \Sigma_A^\mp$ (e.g., Neubauer, 1998). In the latter scenario, the displaced wake would disappear and a "classical" absorption wake would be formed in the moon's downstream hemisphere (similar to, for example, Tethys or Rhea, see Simon et al., 2009; Simon et al., 2012). The lower the interaction strength, the closer the displaced wake (green in Figure 1) would be to the geometric one (red).

Using $\tilde{x} = \tilde{r} \cos \tilde{\phi}$ and $\tilde{y} = \tilde{r} \sin \tilde{\phi}$, the partial derivatives of the potential in Equations 3–5 are both constant inside the wing tubes ($\tilde{r} \leq R$): $\partial_{\tilde{x}} \psi^\mp = 0$ and $\partial_{\tilde{y}} \psi^\mp = E_0 \alpha^\mp$. Inserting these values into the equations for the magnetic field and using Equation 9 for the flow velocity then yields the following expression for the (constant) velocity u_z^- inside of the $z > 0$ (upstream) wing in Triton Interaction coordinates (x, y, z):

$$u_z^- = \frac{B_0 \cos \vartheta \left\{ -\sqrt{1 + M_A^2 - 2M_A \sin \vartheta - M_A^2 (\alpha^-)^2 \cos^2 \vartheta} + M_A (\alpha^- - 2) \sin \vartheta + M_A^2 (1 - \alpha^-) + 1 \right\}}{\sqrt{\mu_0 n_0 m} (1 + M_A^2 - 2M_A \sin \vartheta)}. \quad (12)$$

An expression for the critical angle ϑ_c can be found by setting the term inside of the curly brackets to zero, which yields a quadratic equation for $\sin \vartheta_c$:

$$\sin^2 \vartheta_c - \frac{1 - M_A^2 (\alpha^- - 2)}{2M_A} \sin \vartheta_c - \frac{(1 + M_A^2) (\alpha^- - 1)}{4} = 0. \quad (13)$$

One solution of this equation,

$$\sin \vartheta_c = \frac{1 + M_A^2}{2M_A}, \quad (14)$$

does *not* fulfill the $\sin \vartheta_c \leq 1$ condition. The other solution provides a very compact equation that expresses ϑ_c in terms of the Alfvénic Mach number and the interaction strength:

$$\sin \vartheta_c = \frac{1}{2} M_A (1 - \alpha^-) = \frac{1}{2} M_A \lambda^-. \quad (15)$$

However, the \underline{z}^- characteristic does not rotate from Triton's downstream ($x > 0$) into its upstream ($x < 0$) hemisphere until $\tan \vartheta > \tan \vartheta_A^-$. According to Equation 2, this condition is fulfilled when $\sin \vartheta \geq M_A$, yielding an angle ϑ_c larger than the value from Equation 15. In other words, the sign of u_z^- flips while both Alfvén wings are still oriented toward downstream. Thus, a "conservative" estimation for the critical angle is

$$\sin \vartheta_c = M_A. \quad (16)$$

Once ϑ exceeds this threshold, one can be sure that the \underline{z}^- characteristic penetrates into the upstream hemisphere *and* the flow in that wing is deflected antiparallel to the z axis.

Values of the Alfvénic Mach number along Triton's orbit range from $M_A = 0.22$ (or even lower) up to $M_A = 0.35$ (Liuzzo et al., 2021). Therefore, the displaced wake can appear for angles ϑ exceeding $\vartheta_c \approx 13^\circ$ – 20° . Thus, the formation of this structure requires only a rather minor deviation from the $\underline{u}_0 \perp \underline{B}_0$ case, that is, it may occur along extended segments of Triton's orbit (see Figure 1 of Liuzzo et al., 2021). We therefore suggest that the displaced wake is a persistently observable feature of this moon's plasma interaction.

For different values of λ^\mp , Figures 4a and 4b illustrate the dependence of the (constant) velocity u_z^\mp within the upstream (Equation 12) and downstream wings on the angle ϑ . The velocity within the downstream wing tube reads

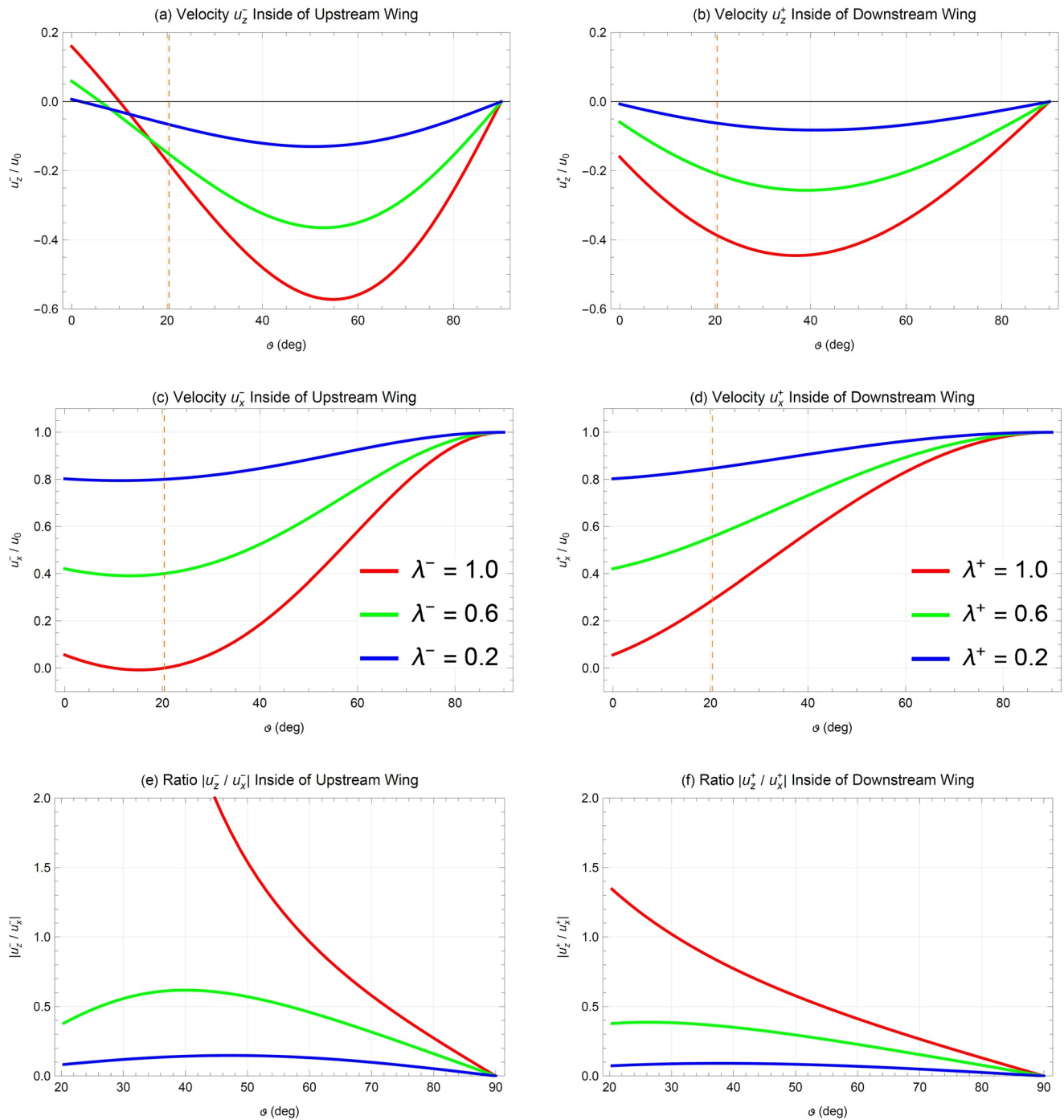


Figure 4. Dependence of the velocity components u_z^\mp [in units of u_0 , panels (a) and (b)] and u_x^\mp [panels (c) and (d)] within Triton's upstream-facing and downstream-facing Alfvén wings on the angle ϑ and the strength $\lambda^\mp = \Sigma_p / (\Sigma_p + 2\Sigma_A^\mp)$ of the moon's plasma interaction. The case of $\lambda^\mp \approx 1$ ("saturated" interaction) is most representative of the actual Triton scenario. The dashed orange lines in panels (a)–(d) denote the critical angle $\vartheta_c = \arcsin M_A \approx 20^\circ$ above which both conditions for the formation of the displaced wake are met. The ratio of both velocity components within the upstream and downstream wings (for $\vartheta \geq \vartheta_c$) is displayed in panels (e) and (f), respectively. Please note that the range of the horizontal axis in plots (e) and (f) is different from that in the other four panels.

$$u_z^+ = \frac{B_0 \cos \vartheta \left\{ \sqrt{1 + M_A^2 + 2M_A \sin \vartheta - M_A^2(\alpha^+)^2 \cos^2 \vartheta} + M_A(\alpha^+ - 2) \sin \vartheta + M_A^2(\alpha^+ - 1) - 1 \right\}}{\sqrt{\mu_0 n_0 m} (1 + M_A^2 + 2M_A \sin \vartheta)}. \quad (17)$$

For comparison, the u_x^\mp component (along the upstream flow direction),

$$u_x^\mp = u_0 \pm \frac{B_0 \left\{ (\sin \vartheta \mp M_A) \sqrt{1 + M_A^2 \mp 2M_A \sin \vartheta - M_A^2(\alpha^\mp)^2 \cos^2 \vartheta} \pm M_A \alpha^\mp \cos^2 \vartheta - \sin \vartheta (1 + M_A^2 \mp 2M_A \sin \vartheta) \right\}}{\sqrt{\mu_0 n_0 m} (1 + M_A^2 \mp 2M_A \sin \vartheta)},$$

is displayed in panels 4(c) and (d). The ratio of both components can be seen in panels 4(e) and (f). Due to the absence of the ionospheric Hall effect in the model, u_y^\mp is exactly zero within the wings (see Equations 4 and 9). The magnitude of u_z^\mp increases with the interaction strength. The $u_z^-(\vartheta)$ profile in the upstream wing possesses two roots; one at $\vartheta = \arcsin(M_A \lambda^-/2)$, and the other at $\vartheta = 90^\circ$ [see panel 4(a)]. In the latter case, the Alfvén characteristics \underline{z}^\mp are aligned with the flow axis ($\pm x$), but the convective electric field E_0 vanishes and hence, the wings disappear. The velocity in ($-z$) direction reaches substantial magnitudes of up to $0.6u_0$ in both wings and depends *non-monotonically* on the angle ϑ . In the upstream wing, the strongest flow component in ($-z$) direction occurs around $\vartheta \approx 50^\circ$ – 55° , depending on the interaction strength [see panel 4(a)]. As shown in panel 4(b), the flow in the downstream wing is always directed away from Triton, that is, the only root of $u_z^+(\vartheta)$ can be found at $\vartheta = 90^\circ$. The maximum of $|u_z^+(\vartheta)|$ occurs at a slightly lower angle than in the upstream wing.

The stagnation of the upstream flow within the Alfvén wing tubes is best visible in the u_x^\mp component: the larger the interaction strength, the more significant is the drop of u_x^\mp to velocities far below u_0 (at a given angle ϑ).

Above the critical angle ϑ_c , the u_x^\mp component increases monotonically with ϑ and reaches its maximum $u_x^\mp = u_0$ when \underline{u}_0 and \underline{B}_0 are aligned [see panels 4(c) and (d)]. While the growth of u_x^\mp with increasing ϑ partially "levels off" the enhanced tilt of the velocity vectors that stems from the maximum in $|u_z^\mp(\vartheta)|$, the flow deflection toward Triton in the $z > 0$ half space is most intense for $\vartheta \approx 20^\circ$ – 60° [see panel 4(e)]. Especially, for a saturated interaction ($\lambda^\mp \approx 1$, as is the case at Triton), the ratio $|u_z^-/u_x^-|$ becomes particularly large at angles slightly above $\vartheta = \arcsin M_A$: in this scenario, u_x^- possesses a root at the critical angle. For $\vartheta = \arcsin M_A$, the \underline{z}^- characteristic is perpendicular to the upstream flow direction. Thus, the plasma merely "rains down" onto Triton from $z > 0$, while the flow is strongly deflected away from the moon in the $z < 0$ half space [see panel 4(f)]. When the interaction is saturated, the deflected plasma flows exactly along the Alfvén wing characteristics, that is, the entirety of the flow deflected within the \underline{z}^- wing ultimately hits the obstacle and is absorbed (see Figure 5 and Appendix A). This picture takes into account that the scale height of Triton's atmosphere (which contributes to the radius R of the Alfvénic fluxtubes) is by several orders of magnitude smaller than the radius of the moon (Broadfoot et al., 1989). In the case of a saturated interaction (and in this case only!), the location of the displaced wake can be determined by merely extending the cylindrical \underline{z}^- wing tube into the opposite half space. For the parameters chosen by Liuzzo et al. (2021) in their $\vartheta = 43^\circ$ model scenario, Triton's interaction is close to saturation. This explains why the displaced wake is so well visible in their hybrid simulation.

We also note that the displaced wake *cannot* be refilled by pick-up ions from Triton's ionosphere. Since the field perturbations near the moon are weak, the drift velocity \underline{v}_D of these ions in Triton Interaction coordinates (x , y , z) is approximately given by

$$\underline{v}_D \approx \frac{\underline{E}_0 \times \underline{B}_0}{B_0^2} = \begin{pmatrix} u_0 \cos^2 \vartheta \\ 0 \\ u_0 \sin \vartheta \cos \vartheta \end{pmatrix}. \quad (18)$$

Thus, the pick-up ions move into the $z > 0$ half space, whereas the displaced wake is mainly located at $z < 0$ [see also Figure 7 of Liuzzo et al., 2021].

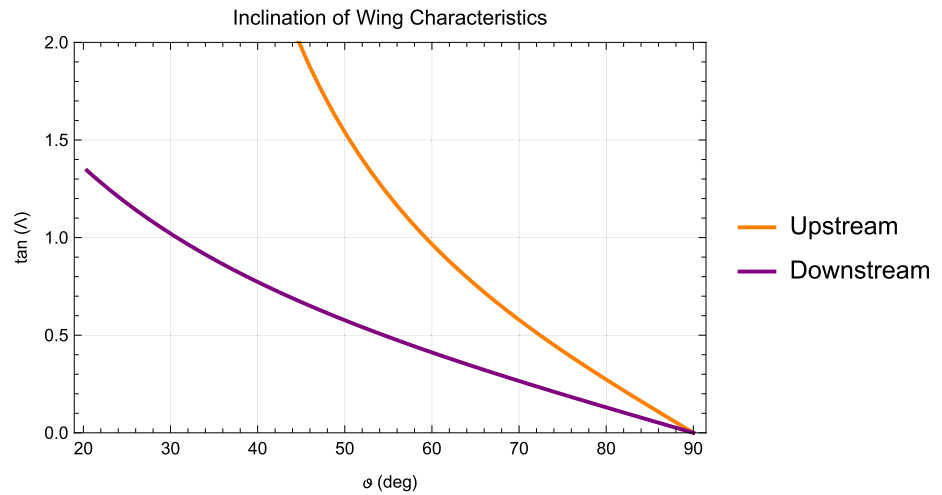


Figure 5. Inclination of the Alfvén wing characteristics against the undisturbed upstream flow direction (+ x), taking into account angles ϑ above the critical angle $\vartheta_c = \arcsin M_A$. For the upstream-facing (orange) and the downstream-facing (purple) wing, the figure displays $\tan(\Lambda)$, where $\Lambda \equiv 90^\circ - \vartheta \pm \vartheta_A^\mp$ is the angle between the respective wing characteristic \underline{z}^\mp and the x axis. The two profiles are identical to those obtained for the ratio of the velocity components when the interaction is fully saturated [red in panels 4(e) and (f)]. Thus, the flow vector in both wings is precisely (anti)aligned with the respective characteristic.

Equations 15 and 16 reveal that the u_x^- component switches signs while both wing characteristics still point into Triton's downstream hemisphere (see also Figure 4a). However, as long as the interaction is unsaturated, this deflection does not lead to the formation of a wake cavity: the flow still moves in positive x direction (i.e., toward downstream), and $u_x^- > 0$ clearly exceeds the magnitude of $u_x^- < 0$ (see Figures 4a and 4c). Therefore, the flow continues to move into the $x > 0$ half space and does not "turn back" to impinge onto Triton. In the case of a saturated interaction, u_x^- possesses roots at $\vartheta = \arcsin(M_A/2)$ and $\vartheta = \arcsin M_A$ [red curve in panel 4(c)]. Between these two roots, the sign of u_x^- is negative. For angles $\arcsin(M_A/2) < \vartheta < \arcsin M_A$, the flow within the \underline{z}^- wing tube would therefore travel "backward" and precisely antiparallel to the \underline{z}^- characteristic. Thus, the plasma would ultimately be absorbed at Triton. However, this does not mean that a depletion region would form in the $x < 0$ half space within this narrow range of angles (from $\vartheta = \arcsin(M_A/2) \approx 10^\circ$ to $\vartheta = \arcsin M_A \approx 20^\circ$): the $x < 0$ half space is fully accessible to the undisturbed upstream flow that would refill such a cavity. We also note that our model includes various simplifications, such as the assumption of a "box-like" ionosphere (see also Simon et al., 2021) and the notion of the background field approximately coinciding with the isolines of the electric potential. Therefore, in-situ observations or numerical simulations using a more complex ionosphere model [like the approach of Liuzzo et al. (2021)] are required to determine whether such a "backward" flow pattern actually exists in reality.

Finally, we have a brief look at the case of *negative* ϑ values which may occur at Triton as well (see Liuzzo et al., 2021). In this scenario, the background field \underline{B}_0 still points into the $z < 0$ half space, but unlike in Figure 1, the field vector now possesses a component toward upstream. Therefore, the projection of the upstream flow velocity onto the direction of the background field ($u_0 \sin \vartheta$) is antiparallel to the magnetospheric field lines. Thus, the "effective" group velocity of the Alfvén mode is smaller than $v_{A,0}$ in the \underline{z}^+ wing and exceeds $v_{A,0}$ in the \underline{z}^- wing, that is, the situation is reversed compared to the case of \underline{B}_0 having a component toward downstream. In consequence, and opposite to the scenario from Figure 1, the inclination angle of the \underline{z}^- wing against \underline{B}_0 is now smaller than the inclination angle of the \underline{z}^+ wing. We find

$$\tan \vartheta_A^\mp = \frac{M_A \cos |\vartheta|}{1 \pm M_A \sin |\vartheta|}. \quad (19)$$

In this scenario, the \underline{z}^+ wing can penetrate into the upstream hemisphere, if the condition

$$\tan \vartheta_A^+ > \tan |\vartheta| \quad (20)$$

is met. This leads to the same expression for the critical angle ϑ_c as in the case of *positive* ϑ values:

$$\sin |\vartheta_c| = M_A. \quad (21)$$

At $\vartheta = \vartheta_c$, the \underline{z}^+ wing is perpendicular to the upstream flow direction. The second condition for the formation of a displaced wake in the $z > 0$ half space now reads $u_z^+(\vartheta) > 0$. Replacing ϑ in Equation 17 with $(-\vartheta)$ and comparing to Equation 12 reveals that the reversal in the sign of $u_z^+(\vartheta)$ occurs at the same angle as in the case of ϑ being positive:

$$\sin |\vartheta| = \frac{1}{2} M_A \lambda^+. \quad (22)$$

Thus, the conditions for the onset of displaced wake formation are the same for the background field having a component toward upstream or downstream. The location of the displaced wake merely switches from the $z < 0$ into the $z > 0$ half space. The angles between \underline{B}_0 and the two Alfvén characteristics also switch between both wings, such that the tilt of the upstream wing against the background field is always larger than that of the downstream wing. However, it is still *not* possible to introduce a mirror plane in Figure 1 that would precisely map, for example, the interaction features from the $z < 0$ hemisphere into the $z > 0$ hemisphere and vice versa when the orientation of the $B_{0,x}$ component changes from downstream to upstream: the background field vector itself is *not* mirrored, that is, it always points into the $z < 0$ half space.

5. Summary and Concluding Remarks

Based on an analytical model, we have studied the deflection of Neptune's magnetospheric plasma near Triton's Alfvén wings. The model captures the (incompressible) perturbations in the Alfvénic far field where the contributions of local ionospheric currents to flow deflection and magnetic field are negligible. Changes in the plasma density near Triton and the associated acceleration of the flow by pressure gradient forces are not taken into account. While the model does not include the ionospheric Hall effect, it does capture the "suspension-bridge"-like Pedersen conductance profile of Triton's ionosphere (Section 3). Our discussion of the critical angle for flow deflection is based on a more simplified approach that treats the moon's ionosphere as a cylinder with uniform Pedersen conductance (Section 4).

For low Alfvénic Mach numbers of the upstream flow and a sufficiently small inclination angle of the magnetospheric field against the upstream flow direction, one of Triton's Alfvén wings may penetrate into the upstream region. We demonstrated that in this case, the incident plasma is deflected toward Triton near the upstream wing and away from the moon near the downstream wing. This asymmetric flow pattern can lead to the formation of a wake cavity that is tilted away from Triton's geometric plasma shadow. Since Triton's interaction is nearly saturated, the flow velocity within both Alfvén wings is aligned with the wing axes. Thus, the upstream wing serves as a "channel" that directs the incident flow toward the moon where it is ultimately absorbed. We found that the displaced wake may be present during extended intervals of Triton's orbit around Neptune.

The notion of a displaced plasma wake at Triton has been put forward by two independent approaches: numerical hybrid simulations (Liuzzo et al., 2021) and analytical work, starting from first principles. However, since the tour of the Voyager 2 spacecraft did not include any close Triton flybys, the existence of such a structure currently remains within the realm of theory. Nonetheless, our work suggests that future missions to the Neptune-Triton system may be able to reveal fundamentally new interaction signatures that do not occur, for example, at the Galilean moons. Indeed, the mechanism proposed here should be observable at numerous moons of Uranus and Neptune: the displaced wake can form whenever an obstacle is exposed to a flow with low M_A and sufficiently small tilt of the upstream velocity against the magnetospheric field (see, e.g., Connerney et al., 1987; Connerney et al., 1991). We emphasize that a moon generating this kind of interaction is not required to possess a dense ionosphere: if the ambient magnetic field is not too strong, even a pure plasma absorber triggers Alfvén wings (Simon et al., 2012). Therefore, the ice giant magnetospheres provide formidable "plasma laboratories" to study this novel type of moon-magnetosphere interaction.

Titan is the only moon in the outer solar system that was already visited by spacecraft and may occasionally fulfill Condition (16) for the onset of displaced wake formation. During the few Titan flybys where a complete set of upstream parameters could be obtained from Cassini observations, the moon was exposed to a *super*-Alfvénic

magnetospheric plasma (e.g., Neubauer et al., 2006; Kallio et al., 2007). However, there is evidence that the Alfvénic Mach number along Titan's orbit can drop to as low as $M_A = 0.28$ (see Table 6 of Arridge et al., 2011). Thus, a deviation of only $\vartheta_c \approx 16^\circ$ from the $\underline{u}_0 \perp \underline{B}_0$ scenario would be sufficient to initiate, for example, southward flow deflection in the moon's northern Alfvén wing. This condition on the field inclination alone was met during an overwhelming number of Cassini flybys (Kabanovic et al., 2017; Simon et al., 2010; Simon, van Treeck, et al., 2013). However, apart from the absence of flyby-to-flyby information on the value of M_A , most of Cassini's upstream encounters occurred at altitudes below one moon radius (Simon et al., 2015). Therefore, the spacecraft may not have intersected the region where the flow in a possible upstream wing is deflected toward Titan. Besides, the moon's environment is perturbed by strongly variable (and so far, largely unpredictable) magnetospheric upstream conditions, evolving on time scales that range from minutes to hours (Simon et al., 2010). Titan's exposure to such a highly dynamic environment may render the identification of a displaced wake cavity infeasible. Besides, this kind of wake signature cannot occur at the Terrestrial moon or any other body that is exposed to a highly super-Alfvénic plasma flow ($M_A \gg 1$): in this case, the Alfvén conductance becomes zero and no Alfvén wings are formed. However, the displaced plasma wake may be an ubiquitous feature of the sub-Alfvénic interaction between exoplanets and their host stars (e.g., Saur et al., 2013).

Appendix A: Flow Deflection for a Saturated Interaction

As shown in Figures 4 and 5, when the interaction is saturated ($\alpha^\mp = 0$) the deflected flow in both wings moves precisely along the Alfvén characteristics \underline{z}^\mp . In particular, this means that the entirety of the flow deflected inside of the \underline{z}^- wing tube is channeled toward Triton and ultimately absorbed. Here we demonstrate analytically that in the case of a saturated interaction, the flow velocity within the wing tubes is perfectly (anti)aligned with the respective characteristic.

For $\alpha^\mp = 0$, the components of the bulk velocity within the wing tubes read

$$u_z^\mp = \pm \frac{B_0 \cos \vartheta}{\sqrt{\mu_0 n_0 m}} \cdot \frac{\sqrt{1 + M_A^2 \mp 2M_A \sin \vartheta} - 1}{\sqrt{1 + M_A^2 \mp 2M_A \sin \vartheta}} \quad (\text{A1})$$

and

$$u_x^\mp = \frac{B_0}{\sqrt{\mu_0 n_0 m}} \cdot \frac{\left(\sqrt{1 + M_A^2 \mp 2M_A \sin \vartheta} - 1 \right) (M_A \mp \sin \vartheta)}{\sqrt{1 + M_A^2 \mp 2M_A \sin \vartheta}}, \quad (\text{A2})$$

respectively. Hence, we find

$$\left| \frac{u_z^\mp}{u_x^\mp} \right| = \frac{\cos \vartheta}{\sin \vartheta \mp M_A} \quad (\text{A3})$$

for $\vartheta > \vartheta_c = \arcsin M_A$. The angle between the upstream flow direction (+x) and the Alfvén characteristics (see Figure 5) can be expressed as

$$\tan(90^\circ - \vartheta \pm \vartheta_A^\mp) = \frac{\cos(\vartheta \mp \vartheta_A^\mp)}{\sin(\vartheta \mp \vartheta_A^\mp)}. \quad (\text{A4})$$

Making use of

$$\sin(\vartheta \mp \vartheta_A^\mp) = \frac{\sin \vartheta \mp M_A}{\sqrt{1 + M_A^2 \mp 2M_A \sin \vartheta}} \quad (\text{A5})$$

and

$$\cos(\vartheta \mp \vartheta_A^\mp) = \frac{\cos \vartheta}{\sqrt{1 + M_A^2 \mp 2M_A \sin \vartheta}} \quad (\text{A6})$$

then yields

$$\tan(90^\circ - \vartheta \pm \vartheta_A^\mp) = \frac{\cos \vartheta}{\sin \vartheta \mp M_A}. \quad (A7)$$

Expressions A3 and A7 for the angle against the upstream flow direction are identical.

Data Availability Statement

The work presented in this manuscript is based on purely analytical (“with paper and pen”) calculations, that is, we did not produce any data sets. The plots shown in Figures 2, 4, and 5 have been generated using the *Wolfram Mathematica* software. All plotting routines and visualizations are embedded in the *Mathematica* scripts, an annotated version of which can be downloaded at <https://doi.org/10.5281/zenodo.5090898>.

Acknowledgments

The authors acknowledge financial support from NASA’s *Solar System Workings* program (grants 80NSSC20K0463 and 80NSSC21K0152). The authors are grateful to Fritz M. Neubauer (University of Cologne, Germany) for providing profound and extremely helpful insights into his theory of sub-Alfvénic moon-magnetosphere interactions.

References

- Arridge, C. S., André, N., Bertucci, C. L., Garnier, P., Jackman, C. M., Németh, Z., et al. (2011). Upstream of Saturn and Titan. *Space Science Reviews*, 162(1–4), 25–83. <https://doi.org/10.1007/s11214-011-9849-x>
- Bagenal, F., & Dols, V. (1989). The space environment of Io and Europa. *Journal of Geophysical Research*, 125(5), e2019JA027485. <https://doi.org/10.1029/2019ja027485>
- Belcher, J. W., Bridge, H. S., Bagenal, F., Coppi, B., Divers, O., Eviatar, A., et al. (1989). Plasma observations near Neptune: Initial results from Voyager 2. *Science*, 246(4936), 1478–1483. <https://doi.org/10.1126/science.246.4936.1478>
- Bertucci, C., Sinclair, B., Achilleos, N., Hunt, P., Dougherty, M. K., & Arridge, C. S. (2009). The variability of Titan’s magnetic environment. *Planetary and Space Science*, 57(14–15), 1813–1820. <https://doi.org/10.1016/j.pss.2009.02.009>
- Blöcker, A., Saur, J., & Roth, L. (2016). Europa’s plasma interaction with an inhomogeneous atmosphere: Development of Alfvén Winglets within the Alfvén Wings. *Journal of Geophysical Research*, 121(10), 9794–9828. <https://doi.org/10.1002/2016JA022479>
- Broadfoot, A. A. L., Atreya, S. K., Bertaux, J. L., Blamont, J. E., Dessler, A. J., Forrester, W. T., et al. (1989). Ultraviolet spectrometer observations of Neptune and Triton. *Science*, 246(4936), 1459–1466. <https://doi.org/10.1126/science.246.4936.1459>
- Connerney, J. E. P., Acuña, M. H., & Ness, N. F. (1987). The magnetic field of Uranus. *Journal of Geophysical Research*, 92(A13), 15329–15336. <https://doi.org/10.1029/ja092ia13p15329>
- Connerney, J. E. P., Acuña, M. H., & Ness, N. F. (1991). The magnetic field of Neptune. *Journal of Geophysical Research*, 96(S01), 19023. <https://doi.org/10.1029/91ja01165>
- Hartkorn, O., & Saur, J. (2017). Induction signals from Callisto’s ionosphere and their implications on a possible subsurface ocean. *Journal of Geophysical Research: Space Physics*, 122(11), 11677–11697. <https://doi.org/10.1002/2017ja024269>
- Hess, S. L. G., Delamere, P. A., Dols, V., & Ray, L. C. (2011). Comparative study of the power transferred from satellite-magnetosphere interactions to Auroral emissions. *Journal of Geophysical Research*, 116(A1), A01202. <https://doi.org/10.1029/2010JA015807>
- Kabanovic, S., Simon, S., Neubauer, F. M., & Meeks, Z. (2017). An empirical model of titan’s magnetic environment during the Cassini era: Evidence for seasonal variability. *Journal of Geophysical Research: Space Physics*, 122(11), 11076–11085. <https://doi.org/10.1002/2017ja024402>
- Kallio, E., Sillanpää, I., Jarvinen, R., Janhunen, P., Dougherty, M., Bertucci, C., & Neubauer, F. (2007). Morphology of the magnetic field near titan: Hybrid model study of the Cassini t9 flyby. *Geophysical Research Letters*, 34(24), L24S09. <https://doi.org/10.1029/2007gl030827>
- Khurana, K. K., Russell, C. T., & Dougherty, M. K. (2008). Magnetic portraits of Tethys and Rhea. *Icarus*, 193, 465–474. <https://doi.org/10.1016/j.icarus.2007.08.005>
- Kivelson, M. G., Bagenal, F., Kurth, W. S., Neubauer, F. M., Paranicas, C., & Saur, J. (2004). Magnetospheric interactions with satellites. In F. Bagenal, T. E. Dowling & W. B. McKinnon (Eds.), *Jupiter: The planet, satellites and magnetosphere* (pp. 513–536). Cambridge University Press.
- Kivelson, M. G., Khurana, K. K., & Volwerk, M. (2009). Europa’s interaction with the Jovian magnetosphere. In *Europa*, edited by Robert T. Pappalardo, William B. McKinnon, Krishan K. Khurana; with the assistance of René Dotson with 85 collaborating authors. University of Arizona Press, The University of Arizona space science series. ISBN: 9780816528448, (p. 545).
- Liuzzo, L., Paty, C., Cochran, C., Nordheim, T., Luspai-Kuti, A., Castillo-Rogez, J., et al. (2021). Triton’s variable interaction with Neptune’s magnetospheric plasma. *Journal of Geophysical Research: Space Physics*, 126(11), e2021JA029740. <https://doi.org/10.1029/2021ja029740>
- Liuzzo, L., Simon, S., Feyerabend, M., & Motschmann, U. (2016). Disentangling plasma interaction and induction signatures at Callisto: The Galileo C10 flyby. *Journal of Geophysical Research: Space Physics*, 121(9), 8677–8694. <https://doi.org/10.1002/2016JA023236>
- Majeed, T., McConnell, J. C., Strobel, D. P., & Summers, M. E. (1990). The ionosphere of Triton. *Geophysical Research Letters*, 17(10), 1721–1724. <https://doi.org/10.1029/g1017i010p01721>
- Mejnertsen, L., Eastwood, J. P., Chittenden, J. P., & Masters, A. (2016). Global MHD simulations of Neptune’s magnetosphere. *Journal of Geophysical Research: Space Physics*, 121(8), 7497–7513. <https://doi.org/10.1002/2015ja022272>
- Ness, N., Acuña, M., Burlaga, L., Connerney, J., Lepping, R., & Neubauer, F. (1989). Magnetic fields at Neptune. *Science*, 246(4936), 1473–1478. <https://doi.org/10.1126/science.246.4936.1473>
- Neubauer, F. M. (1980). Nonlinear standing Alfvén wave current system at Io - Theory. *Journal of Geophysical Research*, 85, 1171–1178. <https://doi.org/10.1029/JA085iA03p01171>
- Neubauer, F. M. (1998). The sub-Alfvénic interaction of the Galilean satellites with the Jovian magnetosphere. *Journal of Geophysical Research*, 103, 19843–19866. <https://doi.org/10.1029/97JE03370>
- Neubauer, F. M. (1999). Alfvén wings and electromagnetic induction in the interiors: Europa and Callisto. *Journal of Geophysical Research*, 104(A12), 28671–28684. <https://doi.org/10.1029/1999JA900217>
- Neubauer, F. M., Backes, H., Dougherty, M. K., Wennmacher, A., Russell, C. T., Coates, A., et al. (2006). Titan’s near magnetotail from magnetic field and plasma observations and modelling: Cassini flybys TA, TB and T3. *Journal of Geophysical Research*, 111, A10220. <https://doi.org/10.1029/2006ja011676>
- Saur, J. (2004). A model of Io’s local electric field for a combined Alfvénic and unipolar inductor far-field coupling. *Journal of Geophysical Research*, 109(A1). <https://doi.org/10.1029/2002ja009354>

- Saur, J., Grambusch, T., Duling, S., Neubauer, F. M., & Simon, S. (2013). Magnetic energy fluxes in sub-Alfvénic planet star and moon planet interactions. *Astronomy and Astrophysics*, 552(A119), 1–20. <https://doi.org/10.1051/0004-6361/201118179>
- Saur, J., Neubauer, F. M., & Glassmeier, K.-H. (2010). Induced magnetic fields in solar system bodies. *Space Science Reviews*, 152(1–4), 391–421. <https://doi.org/10.1007/s11214-009-9581-y>
- Saur, J., Neubauer, F. M., & Schilling, N. (2007). Hemisphere coupling in Enceladus' asymmetric plasma interaction. *Journal of Geophysical Research*, 112(A11), A11209. <https://doi.org/10.1029/2007JA012479>
- Saur, J., Neubauer, F. M., Strobel, D. F., & Summers, M. E. (1999). Three-dimensional plasma simulation of Io's interaction with the Io plasma torus: Asymmetric plasma flow. *Journal of Geophysical Research*, 104(A11), 25105–25126. <https://doi.org/10.1029/1999JA900304>
- Simon, S. (2015). An analytical model of sub-alfvénic moon-plasma interactions with application to the hemisphere coupling effect. *Journal of Geophysical Research: Space Physics*, 120(9), 7209–7227. <https://doi.org/10.1002/2015ja021529>
- Simon, S., Boesswetter, A., Bagdonat, T., Motschmann, U., & Schuele, J. (2007). Three-dimensional multispecies hybrid simulation of Titan's highly variable plasma environment. *Annales Geophysicae*, 25(1), 117–144. <https://doi.org/10.5194/angeo-25-117-2007>
- Simon, S., Kriegel, H., Saur, J., & Wennmacher, A. (2013). Energetic aspects of Enceladus' magnetospheric interaction. *Journal of Geophysical Research*, 118(6), 3430–3445. <https://doi.org/10.1002/jgra.50380>
- Simon, S., Kriegel, H., Saur, J., Wennmacher, A., Neubauer, F. M., Roussos, E., et al. (2012). Analysis of Cassini magnetic field observations over the poles of Rhea. *Journal of Geophysical Research*, 117(A7), A07211. <https://doi.org/10.1029/2012JA017747>
- Simon, S., Liuzzo, L., & Addison, P. (2021). Role of the ionospheric conductance profile in sub-Alfvénic moon-magnetosphere interactions: An analytical model. *Journal of Geophysical Research: Space Physics*. <https://doi.org/10.1029/2021JA029191>
- Simon, S., Roussos, E., & Paty, C. S. (2015). The interaction between Saturn's moons and their plasma environments. *Physics Reports*, 602, 1–65. <https://doi.org/10.1016/j.physrep.2015.09.005>
- Simon, S., Saur, J., Kriegel, H., Neubauer, F., Motschmann, U., & Dougherty, M. (2011). Influence of negatively charged plume grains and hemisphere coupling currents on the structure of Enceladus' Alfvén wings: Analytical modelling of Cassini magnetometer observations. *Journal of Geophysical Research*, 116(A4), A04221. <https://doi.org/10.1029/2010JA016338>
- Simon, S., Saur, J., Neubauer, F., Motschmann, U., & Dougherty, M. (2009). Plasma wake of Tethys: Hybrid simulations versus Cassini MAG data. *Geophysical Research Letters*, 36(4), L04108. <https://doi.org/10.1029/2008GL036943>
- Simon, S., Saur, J., Neubauer, F. M., Wennmacher, A., & Dougherty, M. K. (2011). Magnetic signatures of a tenuous atmosphere at Dione. *Geophysical Research Letters*, 38, L15102. <https://doi.org/10.1029/2011GL048454>
- Simon, S., van Treeck, S. C., Wennmacher, A., Saur, J., Neubauer, F. M., Bertucci, C. L., & Dougherty, M. K. (2013). Structure of Titan's induced magnetosphere under varying background magnetic field conditions: Survey of Cassini magnetometer data from flybys TA-T85. *Journal of Geophysical Research*, 118(4), 1679–1699. <https://doi.org/10.1002/jgra.50096>
- Simon, S., Wennmacher, A., Neubauer, F., Bertucci, C., Kriegel, H., Saur, J., et al. (2010). Titan's highly dynamic magnetic environment: A systematic survey of Cassini magnetometer observations from flybys TA–T62. *Planetary and Space Science*, 58(10), 1230–1251. <https://doi.org/10.1016/j.pss.2010.04.021>
- Strobel, D. F., Cheng, A. F., Summers, M. E., & Strickland, D. J. (1990). Magnetospheric interaction with Triton's ionosphere. *Geophysical Research Letters*, 17(10), 1661–1664. <https://doi.org/10.1029/g1017i010p01661>
- Volwerk, M., Khurana, K., & Kivelson, M. (2007). Europa's Alfvén wing: Shrinkage and displacement influenced by an induced magnetic field. *Annales Geophysicae*, 25. <https://doi.org/10.5194/angeo-25-905-2007>